Binary-encounter electron emission after fast heavy-ion impact on complex rare- and molecular-gas targets

U. Bechthold, J. Ullrich, U. Ramm, and G. Kraft
Gesellschaft für Schwerionenforschung m.b.H., Planckstraße 1, D-64291 Darmstadt, Germany

S. Hagmann
J. R. Macdonald Laboratory, Kansas State University, Manhattan, Kansas 66506

D. R. Schultz and C. O. Reinhold
Physics Division, Oak Ridge National Laboratory, Oak Ridge, Tennessee 37831

H. Schmidt-Böcking
Institut für Kernphysik, August-Euler-Straße 6, D-60486 Frankfurt, Germany
(Received 4 December 1997; revised manuscript received 3 March 1998)

Doubly differential cross sections (DDCSs) for electron emission have been measured for collisions of 3.6 MeV/u Ne^{10+}, Xe^{40+} and 5.9 MeV/u U^{29+} on neon, xenon, water, ethanol, methanol, propanol, C_2F_6, SF_6, and C_3F_8. Electrons ejected with emission angles between 0° and 180° with respect to the ion beam axis have been recorded simultaneously using a toroidal electron spectrometer. We analyze the singly differential cross section (SDCS) for binary encounter electron (BE*e*) production as a function of target electron number and laboratory emission angle. We find that there exists a linear scaling of the BE*e* SDCS with the number of electrons bound in the target with an energy lower than the reduced projectile energy. The enhancement of BE*e* production in the forward direction in collisions with partially stripped ions is studied for the different projectiles and targets and compared to theoretical calculations. [S1050-2947(98)06608-6]

PACS number(s): 34.50.Fa, 34.70.+e

I. INTRODUCTION

Because electron production is the principal mechanism responsible for the energy dissipation in heavy-ion collisions with atoms, molecules, and solids, great efforts have historically been made to obtain systematic data on doubly differential electron cross sections. Thus, in addition to furthering the basic understanding of scattering processes in ion-atom collisions, the cross sections measured for collisions of heavy ions with gas targets are used in many applied fields.

Doubly differential electron emission spectra following fast bare heavy ion impact often display three prominent features. First, a peak near zero electron energy is apparent, with the low-energy electron region being dominated by the continuous decrease of electron intensity as a function of increasing electron energy. This so-called ''soft electron peak'' is due to target ionization by peripheral collisions between the projectile ion and the target [1]. Second, ejected electrons that asymptotically travel with nearly the same velocity as the ion beam, $\vec{v} \simeq \vec{v}_p$, where $\vec{v}_p$ and $\vec{v}$ are the projectile and the electron velocities, respectively. Thus, these electrons appear at forward emission angles and at the ''reduced'' energy $E \simeq \epsilon_p = 1/2\ v_p^2$ (atomic units are used throughout, except where explicitly noted). This cusp-shaped feature of the spectrum originates from the electron-capture-to-the-continuum (ECC) process [2,3]. A third feature is the peak due to hard binary collisions of target electrons with the impinging ion, the binary encounter electrons (BE*e*) [4]. Such close collisions between the projectile and quasi-free target electrons give rise to a ridge with a broad energy distribution centered about $E \simeq 4\epsilon_p \cos^2(\vartheta)$. Throughout the paper the notation ϑ will be used for electron ejection angles in the laboratory system, whereas θ is used for the center-of-mass system. For clothed ions, the first and third features give rise to an electron-loss-to-the-continuum (ELC) ridge observed at $E \simeq \epsilon_p$ for all emission angles. The forward ELC cusp is due to peripheral collisions, whereas the backward ELC peak is due to head-on binary collisions between the target core and a projectile electron (i.e., backward BE*e*).

To date, experimental data on electron emission in fast heavy ion collisions with complex molecules are scarce and often suffer by the limited range of observation angles or electron energies for which the measurements were carried out (for a complete review see Refs. [5,6]). Through the present work we add to the available information by studying the scaling behavior of BE*e* emission from multielectron targets heavier than in previous experiments and over a wide range of emission angles ($0° \leqslant \vartheta \leqslant 180°$). Numerous studies for light bare ions revealed that the BE*e* peak may be well described within the framework of a variety of classical, semiclassical, and quantum-mechanical formulations of the elastic scattering of quasifree electrons by the Coulomb potential of the impinging ion [4,7–9]. In particular, the well-known scaling behavior of the BE*e* DDCS with the square of the projectile nuclear charge, Z_P, was established. However, experiments considering BE*e* production for nonbare ions showed that these scaling laws could be applied only at large angles ($\vartheta > 40°$) [10]. In fact, depending on the collision system, BE*e* emission could decrease or increase with decreasing charge state of the projectile [11]. The root of this

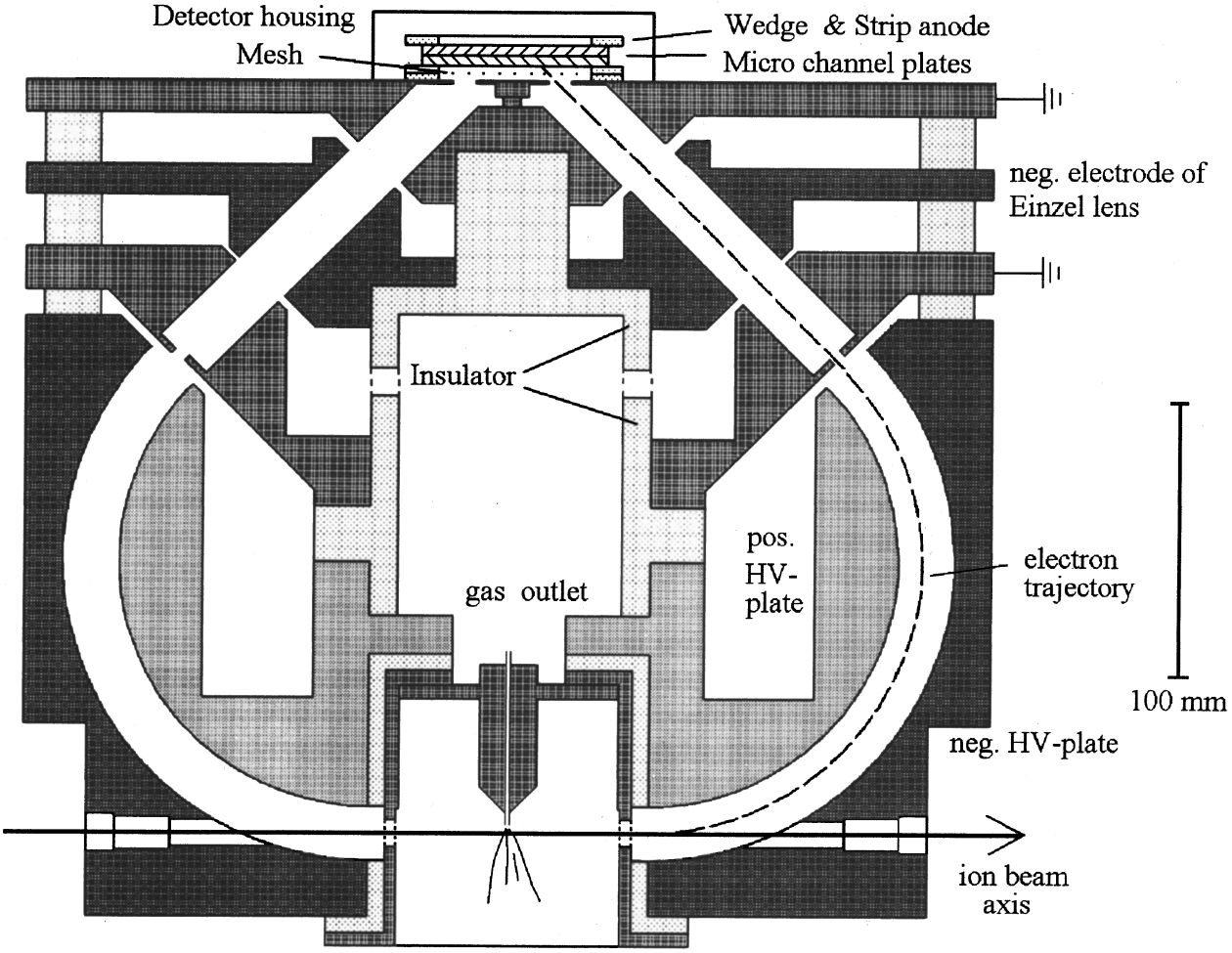

FIG. 1. Schematic drawing of the toroidal electron spectrometer. The spectrometer is rotationally symmetric (360°) around an axis through the gas outlet.

''anomalous'' behavior stems from the characteristics of the elastic scattering cross section of an electron by the clothed ion [12–17]. The effect of this non-Coulomb interaction induced by the partially clothed projectile can be dramatic and can produce diffractive oscillations [13,18], as experimentally confirmed in many cases [13,19–22]. In the present analysis we therefore account for the proper treatment of non-Coulomb interactions. However, owing to the existence of many previous works, we will refrain from lengthy discussion of two-center effects (TCE) in BE*e* emission [23–26] (i.e., interaction of the ejected electron with both the projectile and residual target ions) such as shifts of the BE peak to smaller electron energies. In particular, we focus on the scaling properties of the overall BE*e* emission with respect to the number of electrons in the target and the elastic scattering cross section.

II. EXPERIMENTAL METHOD

In order to enhance detection efficiency over former designs, a toroidal electron analyzer was developed by one of the authors (S.H.). In contrast to the design of conventional spherical analyzers, the electrostatic field of the analyzer is formed by a toroidal geometry of the deflection plates, as shown in Fig. 1. Thus, it is possible to obtain an extended field free target area and, for example, incorporate foil target holders or a TOF recoil ion spectrometer for coincidence experiments.

The projectile ion beams were produced in the ECR source at GSI Darmstadt and accelerated by the UNILAC to 3.6 MeV/u for the Ne and Xe ions and 5.9 MeV/u for the U ion, respectively. The well collimated ion beam enters the spectrometer through a 10-mm hole in the outer negative electrode, interacts with the gaseous target effusing through a 0.7-mm hypodermic needle 4 mm above the beam axis, and leaves through another 10-mm hole. The charged ion beam is collected in a shielded Faraday cup for normalization. The emitted electrons are energy analyzed in the electrostatic field between the two toroidal electrodes. After passing a 3-mm aperture at the exit of the analyzing field, an einzel lens is used for efficient transport of the diverging trajectories onto a microchannel plate (MCP). After amplification by the MCP's, a wedge and strip anode is employed for two-dimensional readout of the position information. A high transmission mesh at a potential of -10 V prevents low-energy electrons from entering the MCP. A subsequent potential of $+200$ V accelerates the electrons onto the MCP's for improved detection efficiency.

The laboratory emission angle is obtained from the position of the electron for each event on the anode relative to the

center of the anode and the direction of the beam axis on the focal ring. The simultaneously observable angular range $\Delta\vartheta$ is therefore 0° to 180° on both sides of the beam axis. Due to the extended source volume, the angular resolution is about 4° in the forward direction and 16° perpendicular to the beam axis. The voltage on the toroidal plates is scanned between 0 and ± 4000 V, corresponding to emission energies between 0 and 20 keV. The energy resolution was determined by the size of the entrance slits in the gas cell, and was set to 8% for the neon and xenon experiments and to 4% for the uranium projectiles. The spectrometer is magnetically shielded by two layers of mumetal, and reliable data are available for energies down to 40 eV. The spectrometer chamber was pumped to 4×10^{-7} mbar during the experiments. Target pressures were in the range of 10^{-4} to 10^{-5} mbar, thus establishing single collision conditions. Beam-induced background electrons produced by scattering of ions by the metal surfaces of collimation slits and spectrometer parts were carefully reduced and measured without target gas for later subtraction. The subtracted background never exceeded about 8–12 % of the total spectrum.

In order to obtain absolute differential cross sections, we normalized the measured DDCS for the bare 3.6 MeV/u Ne^{10+} on Ne 0° binary encounter peak maximum to the one measured by Zouros *et al.* [27], where a 1.875-MeV/u O^{8+} was incident on a neon target. In this collision energy regime the agreement of the impulse approximation with experimental data for BE*e* production at 0° is found to be very good, so that a scaling by the factor Z_P^2/E_P^2 between the two experiments is appropriate, where E_P is the projectile energy in the laboratory frame. The uncertainty introduced by this procedure is expected to be less than 15% and was therefore used for all experiments with the neon and xenon ion beams, that were performed under identical conditions. Normalization of the data obtained with the uranium projectile was undertaken by using the data of Ramm [28], where a 5.9-MeV/u Pb^{26+} projectile was incident on a neon target. Again, the binary encounter peak maximum at 0° was taken as the reference point. To a good degree of approximation, this collision system is very similar to the 5.9-MeV/u U^{29+}-Ne system in our experiment. Nevertheless, due to uncertainties of about 40% in the data of Ramm we expect our data to have the same absolute error.

III. THEORETICAL ANALYSIS OF THE EXPERIMENTAL DATA

A brief synopsis of the theoretical models used to describe BE*e* emission serves to illustrate the physical mechanisms leading to this feature and to explain our analysis of the experimental data.

The simplest theoretical descriptions of BE*e* emission can be traced back to the impulse approximation (IA) [29]. In order to obtain simple expressions, however, most calculations make use of various on-shell approximations to the exact IA [30]. This has lead to a family of approaches that are very similar to each other including the binary encounter method [12,13], the elastic scattering model [7], and some that are also called the impulse approximation [31,32]. The main assumption in these approaches is that during the collision the electron is elastically scattered by the field of the impinging ion while the target core remains as a spectator. Thus, BE*e* DDCSs adopt the form of a convolution between the elastic cross section and the square of the momentum wave function of the target electrons.

The principal ingredient in all on-shell IAs is the differential cross section for scattering of an electron by the projectile field $d\sigma^{\rm el}/d\Omega'_{\rm c.m.}(E'_{\rm c.m.})$, where c.m. refers to the center of mass between the electron and the projectile (for all practical purposes it is equivalent to the projectile reference frame). The various on-shell IA approximations differ from each other in the prescription relating the solid angle and energy entering the elastic cross section, $\Omega'_{\rm c.m.}$ (scattering angle θ'), $E'_{\rm c.m.}=v'^2/2$, with their asymptotic values in a three-body collision $\Omega_{\rm c.m.}$ (scattering angle ϑ), $E_{\rm c.m.}=v^2_{\rm c.m.}/2$. Using the on-shell IA of Ref. [30] the DDCS of electron emission from an initial target state ψ_i is given in the projectile frame by

$$\frac{d^2\sigma}{dE_{\rm c.m.}d\Omega_{\rm c.m.}}=v_{\rm c.m.}\frac{d\sigma^{\rm el}}{d\Omega'_{\rm c.m.}}(E'_{\rm c.m.})\int d\Omega_{v'}|\psi_i(\vec{v}'-\vec{v}_p)|^2, \tag{1}$$

where, in terms of the ionization potential of the electron, U_i,

$$E'_{\rm c.m.}=E_{\rm c.m.}+U_i, \tag{2}$$

$$\sin^2\left(\frac{\theta'}{2}\right)=\sin^2\left(\frac{\theta_{\rm c.m.}}{2}\right)-(v'-v_{\rm c.m.})\cdots\left(\frac{v'+v_{\rm c.m.}-2v'\cos\vartheta}{4E'_{\rm c.m.}}\right). \tag{3}$$

This on-shell IA (and the binary encounter method) differs from that of Ref. [32] in the inclusion of the ionization potential. Clearly, the ionization potential must play a role since the electron has to escape the target field in a three-body collision. The effect is negligible (i.e., $v'\simeq v_{\rm c.m.}$, $\theta'\simeq\theta_{\rm c.m.}$) when the electron energy is much bigger than the ionization potential but, as we shall see below, it cannot be ignored when they become comparable. Finally, the DDCS in the projectile reference frame is related to the DDCS in the laboratory reference frame through the transformation

$$\frac{d^2\sigma}{dE_{\rm c.m.}d\Omega_{\rm c.m.}}=\sqrt{\frac{E_{\rm c.m.}}{E}}\frac{d^2\sigma}{dEd\Omega}, \tag{4}$$

$$E_{\rm c.m.}=E+\epsilon_p-2\sqrt{\epsilon_pE}\cos\vartheta, \tag{5}$$

$$\sqrt{E_{\rm c.m.}}\cos\theta_{\rm c.m.}=\epsilon_p-\sqrt{E}\cos\vartheta. \tag{6}$$

In order to analyze the scaling properties of the overall binary ridge from the measured DDCSs, we define the singly differential cross section (SDCS) for production of binary electron by integration over an electron energy interval ΔE containing the binary peak

$$\left[\frac{d\sigma}{d\Omega}\right]_{\rm BE}=\int_{E^{\max}-\Delta E/2}^{E^{\max}+\Delta E/2}dE\,\frac{d^2\sigma}{dEd\Omega} \tag{7}$$

$$= \int_{E_{\mathrm{c.m.}}^{-}}^{E_{\mathrm{c.m.}}^{+}} dE_{\mathrm{c.m.}} \frac{dE}{dE_{\mathrm{c.m.}}} \sqrt{\frac{E}{E_{\mathrm{c.m.}}}} \frac{d^2\sigma}{dE_{\mathrm{c.m.}} d\Omega_{\mathrm{c.m.}}}, \tag{8}$$

where $E_{\max} = E_{\max}(\vartheta) \simeq 4\epsilon_p \cos^2\vartheta$ is the peak maximum and, from Eq. (5), $dE/dE_{\mathrm{c.m.}} = (1 - \sqrt{\epsilon_p/E}\cos\vartheta)^{-1}$. $E_{\mathrm{c.m.}}^{+}$ and $E_{\mathrm{c.m.}}^{-}$ in the integration limits stand for $E_{\mathrm{c.m.}}^{\max} + \Delta E_{\mathrm{c.m.}}/2$ and $E_{\mathrm{c.m.}}^{\max} - \Delta E_{\mathrm{c.m.}}/2$, respectively. Using a peaking approximation at $E = 4\epsilon_p \cos^2\vartheta$, $E_{\mathrm{c.m.}} = \epsilon_p$, in Eq. (8),

$$\left[\frac{d\sigma}{d\Omega}\right]_{\mathrm{BE}} \simeq \frac{dE}{dE_{\mathrm{c.m.}}} \sqrt{\frac{E}{E_{\mathrm{c.m.}}}} \int_{E_{\mathrm{c.m.}}^{-}}^{E_{\mathrm{c.m.}}^{+}} dE_{\mathrm{c.m.}} \frac{d^2\sigma}{dE_{\mathrm{c.m.}} d\Omega_{\mathrm{c.m.}}} \tag{9}$$

$$= 4\cos\vartheta \left[\frac{d\sigma}{d\Omega_{\mathrm{c.m.}}}\right]_{\mathrm{BE}}, \tag{10}$$

which allows us to define a SDCS cross section for binary electron production in the projectile (c.m.) frame (the frame transformation essentially agrees with that for Auger lines [33]). Using the same peaking approximation for the integral over $E_{\mathrm{c.m.}}$ and Eq. (1), one should expect that this SDCS scales as

$$\left[\frac{d\sigma}{d\Omega_{\mathrm{c.m.}}}\right]_{\mathrm{BE}} \simeq C_i \frac{d\sigma^{\mathrm{el}}}{d\Omega_{\mathrm{c.m.}}}(\epsilon_p), \tag{11}$$

where the constant C_i should be very close to unity since

$$C_i \simeq \int dE_{\mathrm{c.m.}} v_{\mathrm{c.m.}} \int d\Omega_{v_{\mathrm{c.m.}}} |\psi_i(\vec{v}_{\mathrm{c.m.}} - \vec{v}_p)|^2 \tag{12}$$

$$= \int d^3 v_{\mathrm{c.m.}} |\psi_i(\vec{v}_{\mathrm{c.m.}} - \vec{v}_p)|^2 \simeq 1. \tag{13}$$

In other words, the SDCS for BE*e* emission in the projectile frame should be very similar to the elastic differential cross section. In turn, the laboratory SDCS should scale as

$$\left[\frac{d\sigma}{d\Omega}\right]_{\mathrm{BE}} \simeq 4C_i \cos\vartheta \frac{d\sigma^{\mathrm{el}}}{d\Omega_{\mathrm{c.m.}}}(\epsilon_p). \tag{14}$$

In the next section we test the validity of this approximate scaling. To this end, the experimental SDCSs are directly compared with calculations of the elastic scattering cross sections. For bare projectiles, we can use

$$\frac{d\sigma^{\mathrm{el}}}{d\Omega_{\mathrm{c.m.}}}(\epsilon_p) = \frac{Z_P^2}{\epsilon_p^2 \sin^4(\theta_{\mathrm{c.m.}}/2)}. \tag{15}$$

For non-Coulomb interactions we calculate the cross section using a standard phase-shift approach (see, e.g., [14] for details). The contribution of each substate i with a different Compton profile in the target atom cannot be distinguished in the experimental data, which contains the sum over all target orbitals (i.e., C_i should be replaced by $\Sigma_i C_i$). Nevertheless, one important question arises, which we address in the following section: Is it possible to make a general prediction as to the scaling properties of the constant $\Sigma_i C_i$ for different targets? That is, how close is it to the total number of electrons?

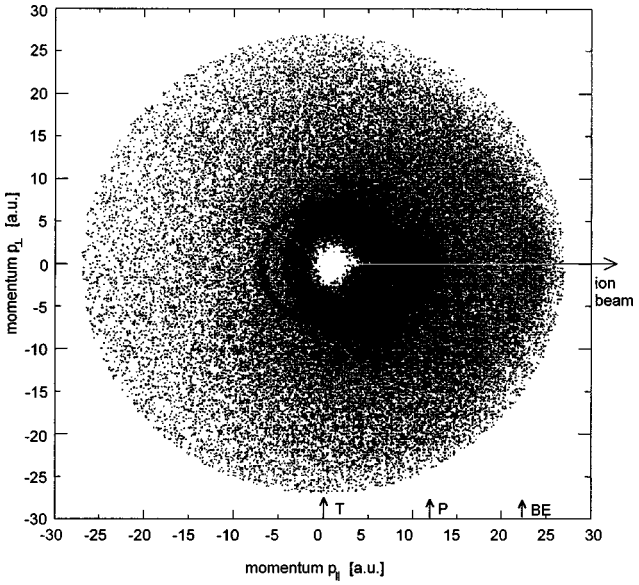

FIG. 2. Scatter plot of the complete final state continuum electron momentum space for the collision system 3.6-MeV/u Ne^{10+} on C_2F_6. *T* and *P* denote the center of the target system and the projectile system. The TCE emission intensity is set to zero if the number of counts exceed an arbitrary value in $p_\parallel$ and $p_\perp$ resulting in a white ''blot'' at the origin, where most of the counts are due to soft and TCE electron emission in the target frame.

IV. RESULTS AND DISCUSSION

A. BE electron production in collisions with 3.6-MeV/u Ne^{10+}

The complete two-dimensional final-state momentum spectrum resulting from a collision of a bare ion (3.6-MeV/u^{20} Ne^{10+}) with a molecular gas target (C_2F_6) is presented in Fig. 2. The momenta are given in atomic units for the momentum components parallel ($v_\parallel$) and perpendicular ($v_\perp$) to the beam direction on the *x* axis and *y* axis, respectively. The scattering angle ϑ is calculated by $\tan(\vartheta) = (v_\perp/v_\parallel)$. The density of the points is proportional to $\log_{10}(d^2\sigma/d\Omega dv)$. The values are cut off for large numbers of counts, for improved visibility of low intensity structures of the spectrum, and are thus responsible for the white area around $(v_\parallel, v_\perp) = (0,0)$. The unusual presentation in the form of a momentum spectrum is chosen to emphasize the three common structures of the emission spectrum described in the Introduction.

Specifically, low-energy, target-centered electron emission is localized around (0,0). Owing to the postcollisional interaction of the slow electron with the receding projectile ionic charge, their intensity is slightly shifted into the forward emission half sphere. These electrons are influenced by both the projectile as well as the target potential, resulting in ''two-center-effects'' (TCE) on the electron emission characteristics [34–37]. In the forward direction (0°) at $\vec{v} = (12,0) \simeq \vec{v}_p$, the peak structure originates from the ECC process. The binary encounter (BE) ridge forms a broad ring-shaped distribution with a radius of ~12 a.u., centered at about $\vec{v} = (12,0)$, resulting in a maximum velocity of $\sim 2v_p$. The rings around $\vec{v} = (0,0)$ with discrete radii of 4 and 7 a.u. are the target carbon and fluorine *KLL* Auger electron emission and are discernible from the background of

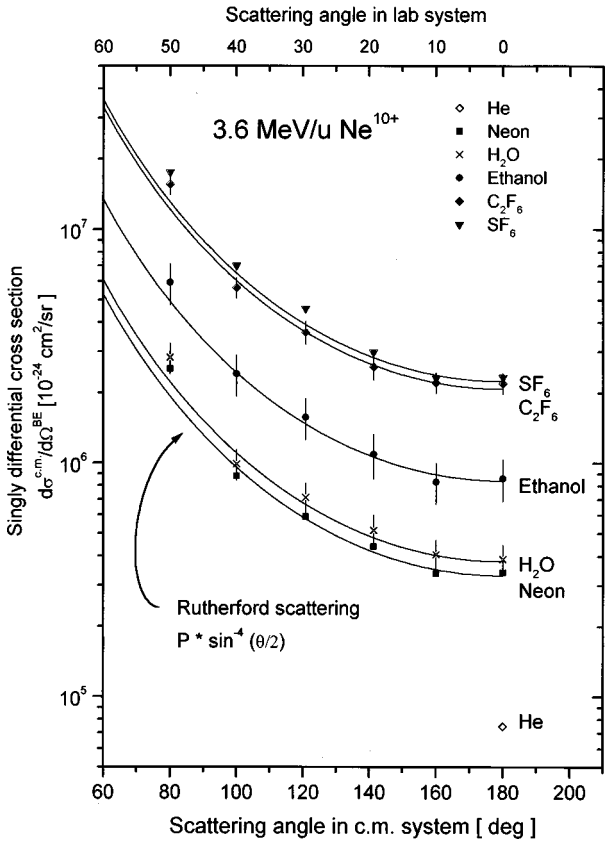

FIG. 3. Singly differential cross section for binary encounter electron production in the c.m. system for 3.6-MeV/u Ne^{10+} on various molecular and rare gas targets. The open diamond indicates the identical experimental [38] and theoretical (IA) SDCS for a helium target [32] .

TCE electrons only in the backward direction.

Figure 3 shows the singly differential cross section of BE*e* emission in the projectile (c.m.) system for various targets in collisions with 3.6-MeV/u Ne^{10+}. The emission is integrated over $\Delta E = 3000$ eV centered around the maximum of the BE peak and therefore ensuring that the complete BE emission is included, and thereby suppressing the variations in the Compton profile of the shells of the wide range of targets, for ease of comparison.

In this case, since BE emission takes place through the scattering of an electron off a bare projectile, the corresponding Rutherford scattering cross section by a pointlike potential is plotted as a line for each target for comparison. The $\sin^{-4}(\theta_{\mathrm{c.m.}}/2)$ dependence of the emission cross section is perfectly reproduced for angles θ larger than 100°. Below this angle the measured cross section is larger than the one predicted by pure Rutherford scattering. This contribution comes from TCE electrons that are not separately discernible at these angles, and were not subtracted. As Ramm [38] showed for bare projectiles from $Z_P = 1$ to 18 in the collision energy regime of 1.5–6 MeV/u, the scaling behavior of the singly differential cross section agrees perfectly with ϵ_p^2/Z_p^2. The predicted BE*e* SDCS from a calculation in the IA is scaled to our collision energy and projectile Z_P and is presented as a diamond in Fig. 3. Furthermore, from our measurements, we can deduce the scaling behavior of the differential cross section with the number of target electrons, as shown in Table I.

TABLE I. Dependence of the single differential BE*e* emission cross section at $\theta = 180°$ from the number of target electrons in the collision system 3.6-MeV/u Ne^{10+} on H_2 [8], He [35], Ne, H_2O, C_2H_5OH, C_2F_6, and SF_6.

Target	N_T^{e-}	$\frac{d\sigma}{d\Omega}(10^{-18}\,\mathrm{cm^2/sr})$	$\frac{d\sigma}{d\Omega}/N_T^{e-}$
H_2, He	2	0.075(1)	0.038(1)
Neon	10	0.33(4)	0.033(4)
H_2O	10	0.38(6)	0.038(6)
C_2H_5OH	26	0.84(9)	0.032(6)
C_2F_6	66	2.08(2)	0.032(3)
SF_6	70	2.24(2)	0.032(3)

The BE*e* SDCSs scale within a deviation of less than 10% with the number of target electrons N_T^{e-}. One exception to the rule is the emission cross section for the water vapor target that is about 15% larger than the cross section for the neon target, which has the same number of electrons. We speculate that this enhancement is due to the smaller mean binding energy of all the electrons in the H_2O molecule. From our measurements, using a simple linear regression, the following general scaling law can be derived for BE*e* production after impact of fast, bare ions:

$$\left[\frac{d\sigma}{d\Omega_{\mathrm{c.m.}}}\right]_{\mathrm{BE}e}^{\mathrm{c.m.}} = 4.9\times10^{-21}\frac{Z_P^2 N_T^{e-}}{\epsilon_p^2 \sin^4(\theta_{\mathrm{c.m.}}/2)}\frac{\mathrm{cm}^2}{\mathrm{sr}} \qquad (16)$$

for $1 \leqslant Z_P \leqslant 18$, $2 \leqslant N_T^{e-} \leqslant 70$, if $\epsilon_p > U_i$, $1.5 \leqslant E_P$ MeV/u$\leqslant 6$, and $180° \geqslant \theta \geqslant 100°$ with an absolute error of less than 15%. These values can easily be transformed to the laboratory system using Eq. (14).

B. BE electron production in collisions with 3.6-MeV/u Xe^{40+}

In collisions with a Xe^{40+} projectile, the effects of the screening of the nuclear charge by the remaining 14 electrons in the projectile is detectable at large scattering angles θ. As shown in Fig. 4 the angular dependence of the singly differential cross sections for BE*e* emission in the 3.6-MeV/u^{129} Xe^{40+} system does not simply follow the Rutherford scattering $\sin^{-4}(\theta_{\mathrm{c.m.}}/2)$ law.

The scattering of the target electrons by the non-Coulomb potential of the partially stripped xenon ions leads to an enhancement of BE*e* emission in the range $180° \geqslant \theta_{\mathrm{c.m.}} \geqslant 100°$ and reaches a factor of about 3 for 180° compared to the q_P^2 scaling, q_P being the ionic charge. This behavior is associated with the well-known ''anomalous'' behavior of the binary peak: at very large impact parameters the electron encounters a pointlike Coulomb potential of charge q_P. Thus, the Rutherford description of scattering is applicable below a certain critical angle $\theta_{\mathrm{c.m.}} < \theta_{\mathrm{crit}}$ (according to Refs. [39–41], $\theta_{\mathrm{crit}} \sim$ 100°–120°). At small impact parameters the incoming electron experiences a potential of the full unscreened nuclear charge Z_P. In the impact parameter range of the orbital radii of the electrons the potential shows strong deviations from the Coulombic $(1/r)$ form: it possesses a

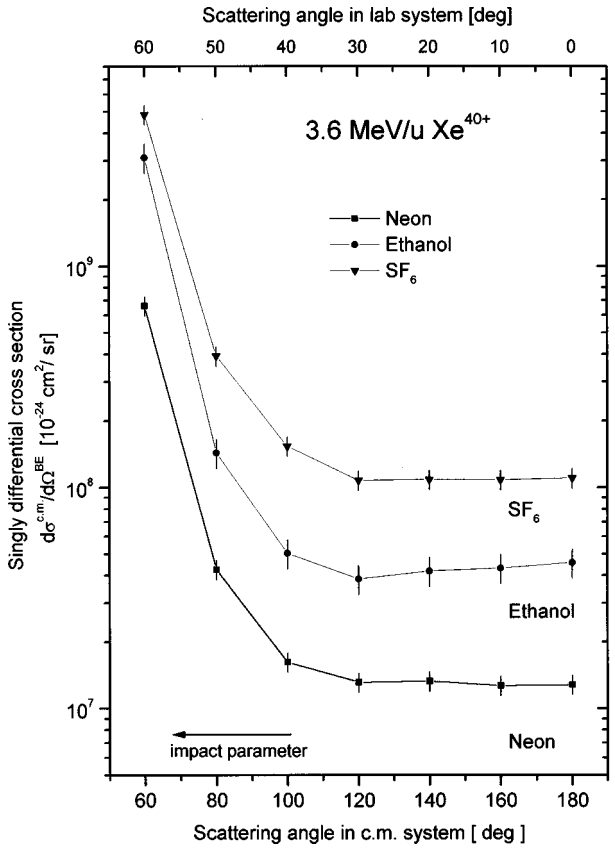

FIG. 4. Singly differential cross section for binary encounter electron production in the c.m. system for 3.6-MeV/u Xe^{40+} on Ne, C_2H_5OH, and SF_6.

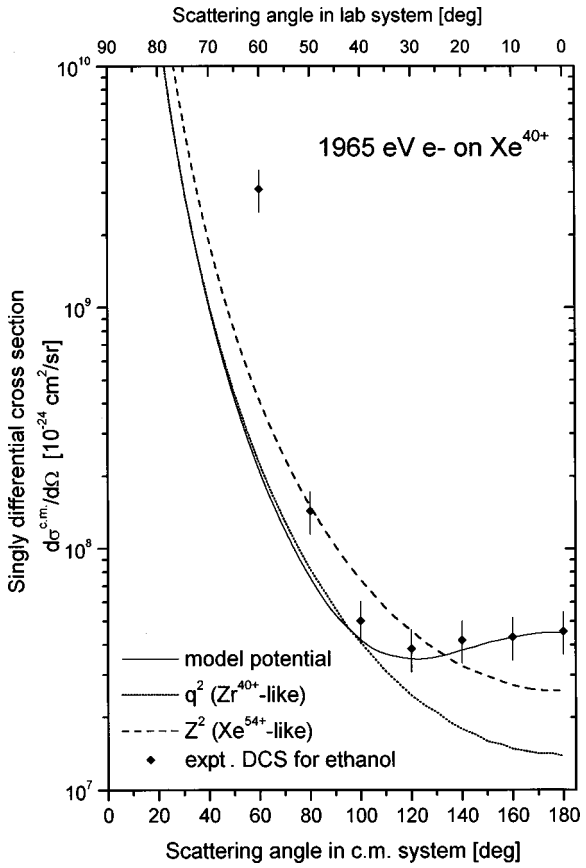

FIG. 5. Comparison of the SDCS for BE*e* production with the elastic cross section for scattering of a 1965-eV electron by a Xe^{40+} projectile. The elastic cross section has been multiplied by the number of active electrons in the ethanol target. Also displayed are the cross sections for fully stripped ions of equal nuclear (Xe^{54+}) and ionic (Zr^{40+}) charge.

stronger gradient $\vec{\nabla} \cdot V(r)$than the potential of a bare nucleus. The momentum exchange in the collision process is proportional to this gradient, therefore the impact parameter range that contributes to the maximum momentum exchange (to $2v_P$) is larger for a screened ion than for a bare ion.

In Fig. 5 we compare the experimental SDCS in the projectile frame with the calculated elastic cross section for 1965-eV electrons impinging on a Xe^{40+} ion and the Rutherford predictions for the according ionic and nuclear charges. The calculations have been multiplied by 26 to account for all the electrons in the ethanol molecule. The agreement between experiment and theory is quite remarkable, implying that the sum $\Sigma_i C_i$ discussed in the theory section is very close to the total number of electrons. At the corresponding angles in the laboratory system the BE electron peak is energetically very well separated from other electron emission processes. The background to the BE*e* peak (ELC, ECC, TCE) has not been subtracted from the measured cross sections. Such a background subtraction has not been attempted because the absolute error introduced by subtracting an exponential fit of the background from the keV broad Gaussian distribution of the binary encounter electrons is rather large. It is therefore not surprising that at small angles the ethanol data lie well above the calculated cross sections.

In Fig. 5 the cross section resulting from the non-Coulomb potential basically agrees with the one from the Rutherford scattering model for a Coulomb potential of strength q_P^2 in the angular range $0° \leqslant \theta \leqslant 100°$. The impact parameter leading to an emission in this angular range is large enough to be outside the screened potential region. The cross section at larger angles in the c.m. system increases to a value in excess of even the one predicted from a Z_P^2 scaling, due to the penetration into the electron cloud of the ion. It has been shown [14] that the enhancement of 180° elastic electron scattering has a maximum that depends strongly on E_P and occurs at energies in the order of 1 to 10 MeV/u ($\epsilon =$ 550 to 5500 eV, respectively) for ions with $Z_P > 26$.

C. BE electron production in collisions with 5.9 MeV/u U^{29+}

In Fig. 6 the two-dimensional, final-state momentum space of electron emission in the collision system 5.9 MeV/u U^{29+} on C_3F_8 is shown. Due to the 63 electrons remaining in the projectile, the screening of the nuclear charge is very strong.

Although soft electron emission is still the dominant process, its intensity in this momentum spectrum is comparable to that of the cusp at $\vec{v} = (15,0)$ and BE electrons at (30,0) near $\vartheta = 0°$. Cross sections of electron production at very low emission energies are mostly influenced by the ionic charge state q_P [28] and do not display the immense effects of projectile screening. Due to the extremely enhanced BE*e* cross section and the large contribution of the cusp electrons the mean energy of electron emission at 0° is of the order of

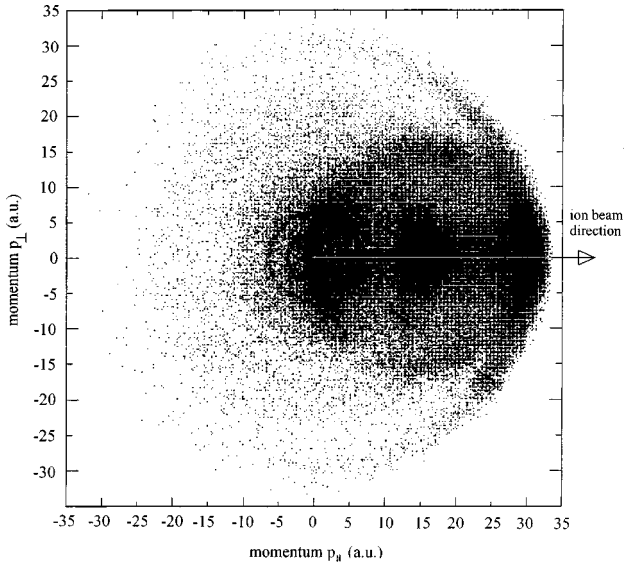

FIG. 6. Complete two-dimensional final-state momentum space for the collision system 5.9-MeV/u U^{29+} on C_3F_8. The straight line at about $\vartheta = -35°$ is caused by a ''hot spot'' on the MCP.

a few keV. ''Walking'' along the BE ridge starting at (30,0) and increasing the emission angle, a reduction in the density is noticeable at about $\vartheta = 25°$. This is caused by a diffractive minimum in the elastic scattering cross section (see Fig. 7). We also note that it has been established [42] that collisions with highly screened heavy ions generally produce a broad target recoil-ion charge state distribution. Since target fluorine *KLL* Auger electrons emitted from different charge states have different energies, the Auger peaks are smeared out, and are not as clearly visible as in Fig. 2 at 4 and 7 a.u. Furthermore, a high energy emission at $v = 2v_P$ is observable at angles ϑ up to 135°, which is the result of an intra-atomic scattering of binary encounter electrons [43]. Experimental SDCS for BE emission in the projectile system for targets with $10 \leqslant N_T^{e^-} \leqslant 90$ are plotted in Fig. 7.

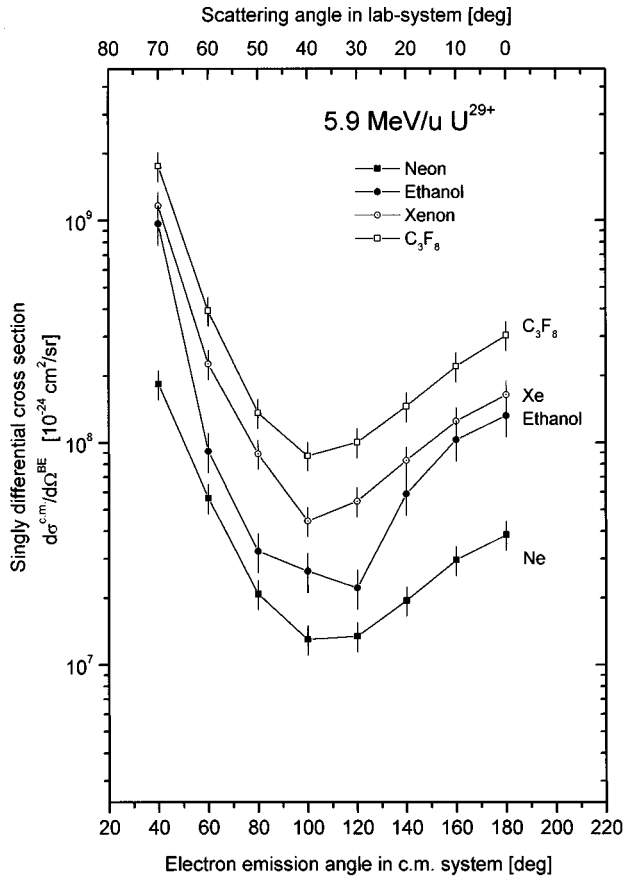

FIG. 7. Singly differential cross section of binary encounter electron production in the c.m. system for 5.9-MeV/u U^{29+} on Ne, ethanol, Xe, and C_3F_8.

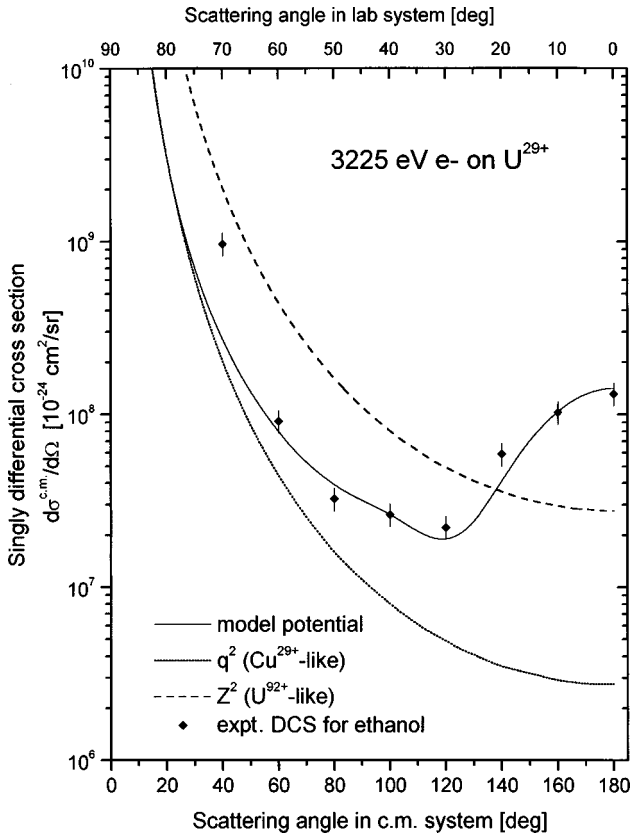

FIG. 8. Comparison of the SDCS for BE*e* production with the elastic cross section for scattering of a 3225-eV electron by a U^{29+} projectile. The elastic cross section has been multiplied by the number of active electrons in the ethanol target. Also displayed are the cross sections for fully stripped ions of equal nuclear (U^{92+}) and ionic (Cu^{29+}) charge.

The strong enhancement over Rutherford cross section is obvious for the large angles in the c.m. system. The cross section for the ethanol target displays a slightly different behavior than the other targets. The enhancement at 180° is stronger and the cross section at small angles in the c.m. system is larger. This is a result of the smaller integration limits ($\Delta E = 3000$ eV) that were used to obtain the differential cross sections. The Compton profiles of the dominant orbitals for BE*e* emission (loosely bound electrons in the outer shells) in the C_2H_5OH molecule are narrower than those for Ne and Xe (and F) atoms, where integration limits $\Delta E = 5000$ eV were used.

Figure 8 shows a comparison of the experimental SDCS and the theoretical result obtained for the corresponding elastic scattering of 3225-eV electrons by the U^{29+} ion. The theoretical data have again been multiplied by 26 to account

TABLE II. Dependence of the single differential BE*e* emission cross section at $\theta = 180°$ from the number of target electrons in the collision system 5.9 MeV/u U^{29+} on Ne, OH_3OH (methanol), C_2H_5OH (ethanol), $CH_3CH(OH)CH_3$ (iso-propanol), and C_2F_6.

Target	N_T^{e-}	$\frac{d\sigma}{d\Omega}(10^{-18}\,\mathrm{cm}^2/\mathrm{sr})$	$\frac{d\sigma}{d\Omega}/N_T^{e-}$
Neon	10	6.4(9)	0.64(8)
CH_3OH	18	11(2)	0.62(9)
C_2H_5OH	26	20(4)	0.77(9)
Propanol	34	24(5)	0.71(9)
Xenon	42 $N_a^{T,e-}$	27(6)	0.65(9)
C_2F_6	66	46(4)	0.70(6)
C_3F_8	90	51(5)	0.60(6)

for the number of electrons in the ethanol molecule.

The agreement between experiment and theory is remarkable down to angles as small as $\theta = 60°$. For $\theta = 180°$ the enhancements over the Rutherford cross section of a bare ion with charge $Z_P = 29$ and over that for bare uranium are factors of 50 and 5.1, respectively. At $\theta = 40°$ the experimental value lies well above the theory, this is again caused by the contribution from other electron emission processes that have not been subtracted.

The measured data follow very well the expected linear scaling with the number of target electrons N_T^{e-} (see Table II). Results for Xe targets, however, exhibit significant deviations from this rule. This can be explained using Bohr's criterion for ionization according to which electrons with an orbital velocity greater than the projectile velocity cannot be ionized. A similar criterion is obtained from Eq. (2) since, in order to emit an electron, its ionization potential must be $U_i < \epsilon_p$. For Xe, there are 12 electrons in the $1s$, $2s$, $2p$, and $3s$ shells whose orbital velocities are greater than the collision velocity [44] and, therefore, play an insignificant role. Remarkably, if one uses the remaining 42 ''active'' electrons to scale the cross section, the agreement with the results for other targets is very good.

V. CONCLUSIONS

We have measured doubly differential cross sections for high-energy binary encounter electron production in fast ion-molecule and ion–rare-gas collisions. The DDCS were integrated over the binary peak energy range in order to analyze its scaling properties. We have shown that the SDCSs are proportional to the differential cross section for elastic scattering by the projectile field. Within small deviations, the singly differential cross section of binary encounter electron emission scales linearly with the number of ''active'' electrons, i.e., electrons with $v_{\mathrm{orb}} < v_P$ (or $U_i < \epsilon_p$). The binary encounter peak is influenced by the projectile structure (i.e., screening), which directly affects the elastic cross section. However, the SDCS for BE*e* emission is nearly independent of the target structure. The magnitude of the momentum and energy transfers required for the production of binary encounter electrons at forward laboratory angles is so large that it suppresses any differences in emission characteristics between rare gas and molecular targets.

ACKNOWLEDGMENTS

U.B., J.U., U.R., G.K., and H.S. are grateful to the BMBF, DFG, GSI, and the European Community for support. S.H. gratefully acknowledges support by the Division of Chemical Sciences, Office of Basic Energy Science, Office of Energy Research, U.S. Department of Energy. D.R.S. and C.O.R. acknowledge the support of the U.S. DOE, Office of Basic Energy Sciences through a grant to ORNL, managed by Lockheed Martin Energy Research Corporation under Contract No. DE-AC05-96OR22464. U.B. would like to acknowledge useful discussions with Professor T.J.M Zouros from the University of Crete.

[1] M. E. Rudd and T. Jorgensen, Jr., Phys. Rev. **131**, 666 (1963).
[2] A. Salin, J. Phys. B **2**, 631 (1969); **5**, 979 (1972).
[3] G. B. Crooks and M. E. Rudd, Phys. Rev. Lett. **25**, 1599 (1970).
[4] T. F. M. Bonsen and L. Vriens, Physica (Amsterdam) **47**, 307 (1970).
[5] N. Stolterfoht, R. D. DuBois, and R. D. Rivarola, *Electron Emission in Heavy Ion-Atom Collisions*, Springer Series on Atoms and Plasmas (Springer, Berlin, 1997).
[6] Author, ICRU-Report No. 55.
[7] D. Bruch, H. Wieman, and W. B. Ingalls, Phys. Rev. Lett. **27**, 1314 (1983).
[8] M. E. Rudd and J. Macek, Case Stud. At. Phys. **3**, 47 (1972).
[9] J. O. P. Pedersen, P. Hvelplund, A. G. Petersen, and P. D. Fainstein, J. Phys. B **24**, 4001 (1991).
[10] L. H. Toburen, N. Stolterfoht, P. Ziem, and D. Schneider, Phys. Rev. A **24**, 1741 (1981).
[11] P. Richard, D. H. Lee, T. J. M. Zouros, J. M. Sanders, and J. L. Shinpaugh, J. Phys. B **23**, L213 (1990).
[12] C. Reinhold, D. R. Schultz, and R. E. Olson, J. Phys. B **23**, L591 (1990).
[13] C. Reinhold, D. R. Schultz, R. E. Olson, C. Kelbch, R. Koch, and H. Schmidt-Böcking, Phys. Rev. Lett. **66**, 1842 (1991).
[14] D. R. Schultz and R. E. Olson, J. Phys. B **24**, 3409 (1991).
[15] K. Taulbjerg, J. Phys. B **24**, L617 (1991).
[16] C. P. Bhalla and R. Shingal, J. Phys. B **24**, 3187 (1991).
[17] H. I. Hidmi, C. P. Bhalla, S. R. Grabbe, J. M. Sanders, P. Richard, and R. Shingal, Phys. Rev. A **47**, 2398 (1993).
[18] C. Reinhold, D. R. Schultz, and R. E. Olson, Nucl. Instrum. Methods Phys. Res. A **56/57**, 271 (1991).
[19] C. Kelbch, R. E. Olson, S. Schmidt, H. Schmidt-Böcking, and S. Hagman, J. Phys. B **22**, 2171 (1989).
[20] W. Wolff, J. L. Shinpaugh, H. E. Wolf, R. E. Olson, J. Wang, S. Lencinas, D. Piscevic, R. Herrmann, and H. Schmidt-Böcking, J. Phys. B **25**, 3683 (1992).
[21] W. Wolff, J. L. Shinpaugh, H. E. Wolf, R. E. Olson, U. Bechthold, and H. Schmidt-Böcking, J. Phys. B **26**, 65 (1993).
[22] S. Hagmann *et al.*, J. Phys. B **25**, 287 (1992).

[23] See, e.g., J. N. Madsen and K. Taulbjerg, J. Phys. B **28**, 1251 (1995).
[24] P. D. Fainstein, V. H. Ponce, and R. D. Rivarola, J. Phys. B **24**, 3091 (1991).
[25] N. Stolterfoht, H. Platten, G. Schiwietz, D. Schneider, L. Gulyas, P. D. Fainstein, and A. Salin, Phys. Rev. A **52**, 3796 (1995).
[26] D. R. Schultz, C. O. Reinhold, and R. E. Olson, *Two-center Effects Ion-Atom Collisions: A Symposium in Honor of M. Eugene Rudd*, edited by T. J. Gay and A. F. Starace, AIP Conf. Proc. No. 362 (AIP, New York, 1996), p. 84.
[27] T. J. M. Zouros, K. L. Wong, S. Grabbe, H. I. Hidmi, P. Richard, E. C. Montenegro, J. M. Sanders, C. Liao, S. Hagmann, and C. P. Bhalla, Phys. Rev. A **53**, 2272 (1996); P. D. Fainstein, V. H. Ponce, and R. D. Rivarola *ibid.* **36**, 3639 (1987); C. O. Reinhold and R. E. Olson *ibid.* **39**, 3861 (1989).
[28] U. Ramm, Dissertation, IKF, University Frankfurt/Main (1994).
[29] F. Drepper and J. S. Briggs, J. Phys. B **9**, 2063 (1976).
[30] Y. Wang, C. O. Reinhold, and J. Burgdörfer, Phys. Rev. A **44**, 7243 (1991).
[31] D. Brandt, Phys. Rev. A **27**, 1314 (1983).
[32] D. H. Lee, P. Richard, T. J. M. Zouros, J. M. Sanders, J. L. Shinpaugh, and H. Hidmi, Phys. Rev. A **41**, 4816 (1990).
[33] N. Stolterfoht, Phys. Rep. **6**, 315 (1987).
[34] R. Moshammer *et al.*, Phys. Rev. Lett. **73**, 3371 (1994).
[35] R. Moshammer, J. Ullrich, H. Kollmus, W. Schmitt, M. Unverzagt, O. Jagutzki, V. Mergel, H. Schmidt-Böcking, R. Mann, C. J. Woods, and R. E. Olson, Phys. Rev. Lett. **77**, 1242 (1996).
[36] M. Unverzagt, R. Moshammer, W. Schmitt, R. E. Olson, P. Jardin, V. Mergel, J. Ullrich, and H. Schmidt-Böcking, Phys. Rev. Lett. **76**, 1043 (1996).
[37] P. Jardin, A. Cassimi, J. P. Grandin, D. Hennecart, and J. P. Lemoigne, Nucl. Instrum. Methods Phys. Res. B **107**, 41 (1996).
[38] U. Ramm, U. Bechthold, O. Jagutzki, S. Hagmann, G. Kraft, and H. Schmidt-Böcking, Nucl. Instrum. Methods Phys. Res. B **98**, 359 (1995).
[39] C. Liao, P. Richard, S. R. Grabbe, C. P. Bhalla, T. J. M. Zouros, and S. Hagmann, Phys. Rev. A **50**, 1328 (1994).
[40] N. Stolterfoht, D. Schneider, D. Burch, H. Wieman, and J. S. Risley, Phys. Rev. A **49**, 5112 (1994).
[41] T. J. M. Zouros, P. Richard, K. L. Wong, H. I. Hidmi, J. M. Sanders, C. Liao, S. Grabbe, and C. P. Bhalla, Phys. Rev. A **49**, R3155 (1994).
[42] J. Ullrich (unpublished).
[43] U. Bechthold, S. Hagmann, J. Ullrich, B. Bathelt, A. Bohris, R. Moshammer, U. Ramm, C. Bhalla, G. Kraft, and H. Schmidt-Böcking, Phys. Rev. Lett. **79**, 2034 (1997).
[44] T. A. Carlson, C. W. Nestor, Jr., N. Wasserman, and J. D. McDowell, At. Data **2**, 63 (1970).